

A general theoretical framework for understanding essential dynamics of Madden–Julian oscillation

Bin Wang^{1,2} · Guosen Chen^{1,2}

Received: 12 March 2016 / Accepted: 7 November 2016 / Published online: 19 November 2016
© The Author(s) 2016. This article is published with open access at Springerlink.com

Abstract Motivated by observed structure of Madden–Julian oscillation (MJO), a general theoretical model framework is advanced for understanding fundamental aspects of MJO dynamics. The model extends the Matsuno–Gill theory by incorporating (a) moisture feedback to precipitation, (b) a trio-interaction among equatorial waves, boundary layer (BL) dynamics, and precipitation, and (c) a simplified Betts–Miller (B–M) cumulus parameterization. The general model with B–M scheme yields a frictionally coupled dynamic moisture mode, which produces an equatorial planetary-scale, unstable system moving eastward slowly with coupled Kelvin–Rossby wave structure and BL moisture convergence leading major convection. The moisture feedback in B–M scheme reinforces the coupling between precipitation heating and Rossby waves and enhances the Rossby wave component in the MJO mode, thereby slowing down eastward propagation and resulting in a more realistic horizontal structure. It is, however, the BL frictional convergence feedback that couples equatorial Kelvin and Rossby waves with convective heating and selects a preferred eastward propagation. The eastward propagation speed in the model is inversely related to the relative intensity of the equatorial “Rossby” westerly versus “Kelvin” easterly associated with the MJO. The cumulus parameterization scheme may affect propagation speed through changing MJO horizontal structure. The SST or

basic-state moist static energy has a fundamental control on MJO propagation speed and intensification/decay. Model sensitivity to BL and cumulus scheme parameters and ramifications of the model results to general circulation modeling are discussed.

Keywords Madden–Julian oscillation · Convectively coupled waves · Frictional convergence feedback · Moisture mode · Moisture feedback · Kelvin waves · Rossby waves

1 Introduction

Notable progress has been made in development of the general circulation models (GCMs), but by far the MJO remains poorly simulated in many GCMs. For instance, the recent assessment of 24 GCMs, which participated in MJOTF (MJO Task Force)/GASS (GEWEX Atmospheric System Study) Global Model Evaluation Project on vertical structure and physical processes of the MJO, reveals that only about one-fourth of the models simulate realistic eastward propagation of the MJO (Jiang et al. 2015). The dynamical models’ prediction skill for the MJO has been rapidly improved, yet remains limited compared to its predictability estimate (Neena et al. 2014; Lee et al. 2015). These indicate the necessity to improve our understanding of the fundamental physics of the MJO.

A variety of theories have been proposed to explain MJO phenomenon over the past two decades, including the wave-CISK (Convective Instability of the Second Kind) (Lau and Peng 1987); the evaporation-wind feedback (Emanuel 1987; Neelin et al. 1987; Wang 1988a); the BL frictional feedback and coupled Kelvin–Rossby wave theory (Wang 1988b; Wang and Rui 1990a; Wang and Li 1994;

✉ Bin Wang
wangbin@hawaii.edu

¹ Department of Atmospheric Sciences and International Pacific Research Center, School of Ocean and Earth Science and Technology, University of Hawaii at Manoa, Honolulu, HI 96822, USA

² Earth System Modeling Center, Nanjing University of Information Science and Technology, Nanjing, China

Kang et al. 2013); the moisture mode theory (Raymond and Fuchs 2009; Sobel and Maloney 2012, 2013; Benedict et al. 2014; Adames and Kim 2015); the MJO skeleton driven by synoptic wave activity (Majda and Biello 2004; Majda and Stechmann 2009); the MJO modified by interactive upscale transfer of eddy momentum, heat and moisture (Wang and Liu 2011; Liu and Wang 2012a, b, 2013); the multi-cloud model of MJO (Khouider and Majda 2006, 2007); the MJO wave packet driven by the interference pattern of a narrow frequency band of mixed Rossby–gravity waves (Yang and Ingersoll 2011) or westward and eastward inertia-gravity waves (Yang and Ingersoll 2013); and the air-sea interaction theory (Flatau et al. 1997; Wang and Xie 1998; Wang and Zhang 2002; Fu and Wang 2004).

In addition to theoretical modeling, various processes and mechanisms have been identified or speculated to play significant roles in MJO dynamics based on numerical model experiences and observations, including shallow convection–BL circulation interaction (Johnson et al. 1999; Kikuchi and Takayabu 2004; Lin et al. 2004); stratiform cloud–wave interaction (Mapes 2000; Khouider and Majda 2006; Kuang 2008; Fu and Wang 2009; Seo and Wang 2010; Holloway et al. 2013); cloud–radiation interaction (Lee et al. 2001; Raymond 2001; Lin and Mapes 2004; Bony and Emanuel 2005; Andersen and Kuang 2012); moisture–convection feedback (Woolnough et al. 2001; Grabowski and Moncrieff 2004; Benedict et al. 2014), and moisture transport (Maloney 2009; Maloney et al. 2010; Andersen and Kuang 2012; Hsu and Li 2012; Kim et al. 2014; Pritchard and Bretherton 2014). More details were reviewed by Zhang (2005) and Wang (2005, 2012).

The diverging views presented above suggest that our knowledge and understanding of the essential dynamics of the MJO remain elusive. A number of critical issues regarding the MJO dynamics remain, particularly: (a) Why does the MJO possess a coupled Kelvin–Rossby wave structure and how could Kelvin and Rossby waves, which propagate in opposite directions, couple together with convection and select eastward propagation? (b) What makes the MJO move eastward slowly (about 5 m/s) over the warm pool, yielding the 30–60 day periodicity? (c) How does SST control the intensification of MJO against dissipation? These are central questions that will be addressed in the present study.

In Sect. 2, observations and model simulations are presented to provide motivation and validation for theoretical models. In Sect. 3, a general MJO framework is formulated that can accommodate different cumulus parameterization schemes. Section 4 demonstrates that the general model can simulate essential features of the MJO and exhibits how MJO-like mode grows/decays over the warm/cold ocean. Section 5 elucidates how the moisture feedback changes MJO structure and propagation speed, and addresses the

mechanisms determining MJO's propagation speed. Section 6 elaborates the critical role of frictional moisture convergence feedback and addresses how the Kelvin and Rossby waves could couple together with convection and select eastward propagation. The last section summarizes the results and discusses the model sensitivity to some critical parameters as well as the ramifications of theoretical results.

2 Observed and model simulated MJO

A question that is important for formulation of theoretical models and validation of MJO theories is: What are the essential features of the MJO that a theory must explain? In this section, we discuss this issue by comparing observations and GCM simulations (Fig. 1). We examined 24 GCMs participated in MJOTF/GASS Global Model Evaluation Project (Jiang et al. 2015). Figure 1 (upper panels) shows propagation and structure of the observed MJO. First, both precipitation and the BL moisture convergence propagate coherently and slowly (about 5 m/s) from 60°E to 170°E with the BL moisture convergence leading precipitation by about 5 days (Fig. 1a). Second, the 850 hPa winds and geopotential field in the tropics exhibit an equatorial Rossby wave (double cyclones) to the west and a Kelvin wave low to the east of the precipitation center, indicating a coupled Kelvin–Rossby wave horizontal structure (Fig. 1b). This confirms the MJO structure documented by Rui and Wang (1990) and Adames and Wallace (2014). Third, the BL Ekman pumping velocity and 700 hPa precipitation heating extend a few thousands of kilometers east of the major precipitation center (Fig. 1c), so that both lead the major precipitation (and the mid-level maximum upward motion). This vertical backward structure is consistent with many previous observational studies (e.g., Sperber 2003; Tian et al. 2006; Jiang et al. 2015).

The aforementioned three observed features are well produced in the good group of GCMs (middle panels) but totally missed in the poor group of GCMs (lower panels). Obviously, the fatal defect of the poor MJO lies in the BL: The BL moisture convergence does not lead major convection and does not propagate eastward. It is also interesting to observe that in the poor group of models, Rossby wave-induced westerly is strong while the Kelvin wave-induced easterly is weak.

Based on the aforementioned observations, we propose that the essential features of the MJO that requests theoretical explanation includes (1) the coupled Kelvin–Rossby wave (horizontal) structure, (2) the slow eastward propagation over the warm oceans (about 5 m/s), (3) the BL moisture convergence and low-pressure leading major convection center, (4) amplification (decay) in the warm (cold)

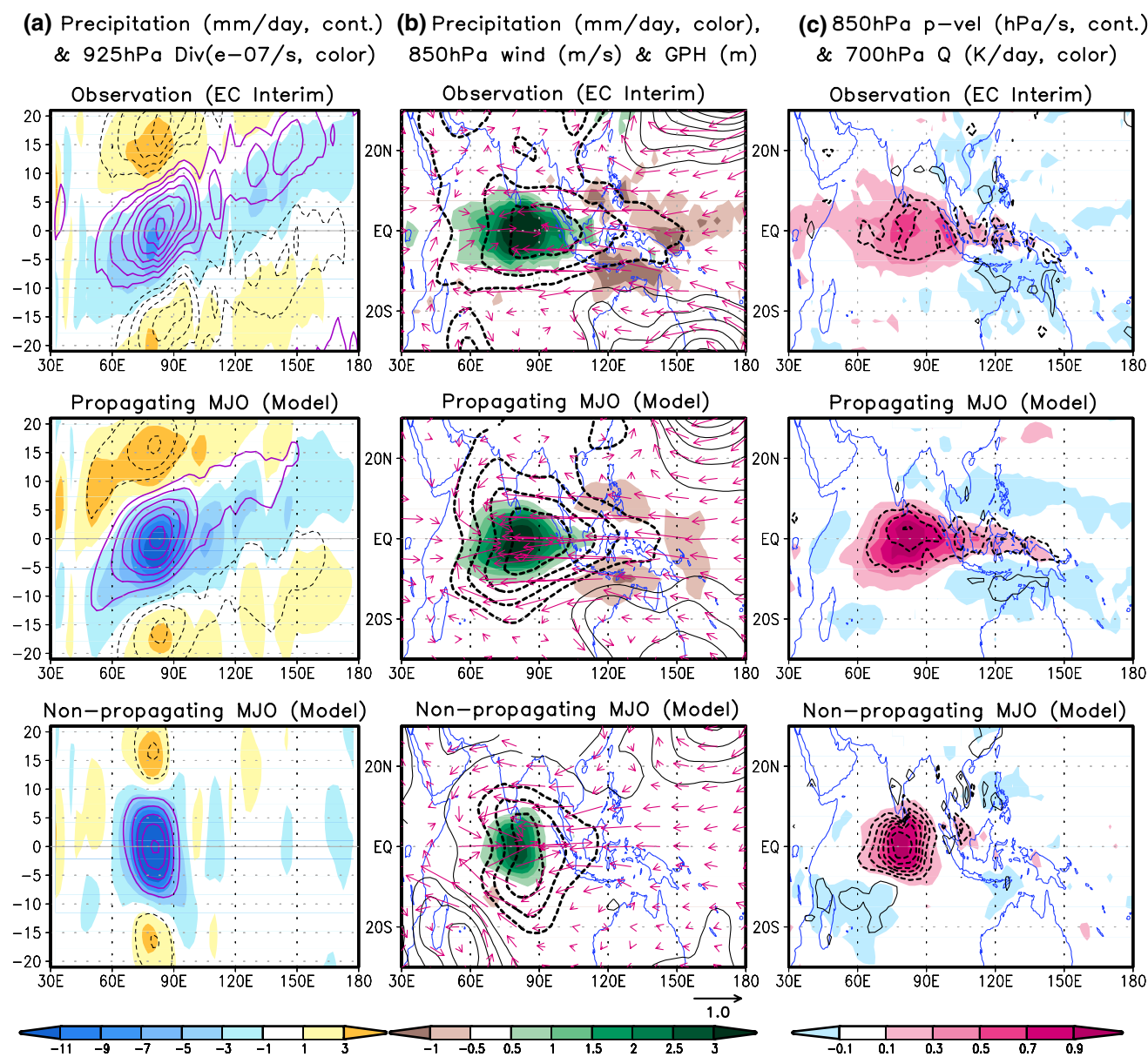


Fig. 1 Observed MJO propagation and structures in comparison with GCM simulated counterparts. **a** *Left column* time-longitude diagram of the regressed precipitation (*contour*) and 925 hPa divergence (*color*) with respect to the MJO precipitation anomalies averaged over the equatorial Indian Ocean (EIO) (5°S–5°N, 70°–90°E). **b** *Central column* Composite 850 hPa winds (*vector*) and geopotential height (*contours*) as well as precipitation (*color shading*) with respect to the EIO precipitation anomalies. **c** *Right column* The same as in (b)

except for 850 hPa vertical p-velocity (*contour*) and 700 hPa diabatic heating (*color*). The models-simulated MJOs were categorized into two groups: good (*middle panels*) and poor (*lower panels*). These two groups of composite maps were made by 7 best propagating models and 7 worst propagating models selected from the 24 GCMs that participate in the MJOTS/GASS global model assessment project (Jiang et al. 2015)

oceans (Madden and Julian 1972), and (5) the planetary zonal circulation scale. These essential features may be viewed as major targets for theoretical interpretation and validation metrics of MJO theory. Note that the feature (1) is indicated by the observation (Fig. 1) and is consistent with previous results in literatures (e.g. Adames and Wallace 2014). However, various theories produce variety

of MJO-like modes with different horizontal structures. Validation of the horizontal structure may test whether a model includes adequate dynamics. Note that the feature (4) implies MJO is an unstable mode, but in some literature MJO is considered as a neutral mode (e.g., Majda and Stechmann 2009; Yang and Ingersoll 2013). Other important features such as the multi-scale convective structure

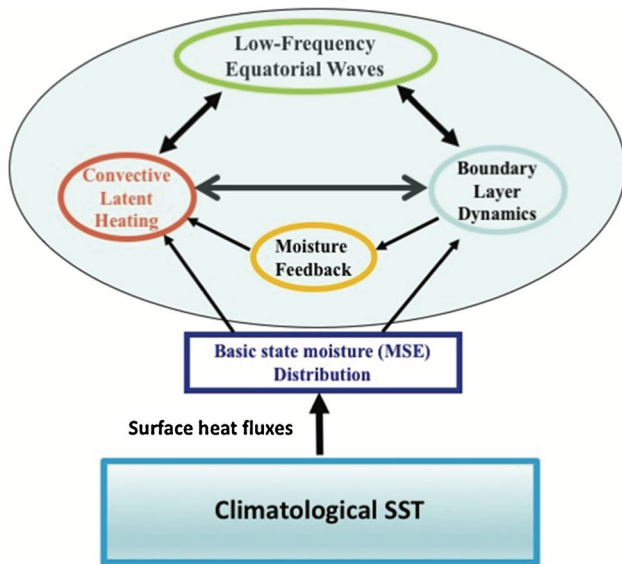


Fig. 2 Schematic diagram illustrating the essential large-scale dynamics of the MJO

(Nakazawa 1988), remarkable seasonal variations (Wang and Rui 1990b), coupling with ocean mixed layer (Krishnamurti et al. 1988), and irregularities (Zhang 2005) should also be explained as higher-level theoretical targets, which require models with higher-level complexity.

3 The general MJO model framework

3.1 The essential model physics

A theoretical model framework should be derived from the first principles with reasonable/justifiable assumptions. The model is designed to include only the essential physical processes that contribute, in a fundamental manner, to MJO dynamics. The coupled convection-Kelvin-Rossby wave structure and the eastward shift of the BL convergence to convective heating implies that the free tropospheric wave dynamics, BL dynamics and interactive heating must be described by the model.

As shown in Fig. 2 the essential process involved in the MJO dynamics is the trio-interactions among free tropospheric large-scale low-frequency waves, BL dynamics, and convective precipitation heating. The complex trio-interaction necessarily involves moist processes, i.e., atmospheric moisture feedback to convective precipitation. The moisture feedback is determined by surface entropy fluxes and the moisture convergence induced by BL dynamics and free tropospheric waves. This model framework can integrate the wave-CISK, wind-evaporation feedback, frictional moisture convergence (FC) feedback,

moisture feedback, as well as wave-activity driven multi-scale interaction mechanisms. In this sense, it is a general model framework that has incorporated ingredients of major existing theoretical models. A unique feature of this model is that the precipitation heat energy comes from the basic state moist static energy, which is largely controlled by basic state SST.

3.2 Non-dimensional governing equations

To describe the free tropospheric, baroclinic equatorial wave motion and BL dynamics, the simplest vertical structure of the model is a 1 and $\frac{1}{2}$ layer equatorial beta-plane model, which consists of the first baroclinic mode in free troposphere and barotropic BL dynamics. Detailed derivation of the model equations is given in the Appendix 1, here we briefly summarize the model equations. Using horizontal velocity scale C_0 , length scale $(C_0/\beta)^{1/2}$, time scale $(\beta C_0)^{-1/2}$, geopotential scale C_0^2 , moisture scale $d_0 \Delta p/g$, where $d_0 = 2p_2 C_p C_0^2 / \Delta p R L_c$, the non-dimensional equations are:

$$\frac{\partial u}{\partial t} - yv = -\frac{\partial \Phi}{\partial x} - vu \quad (1)$$

$$\frac{\partial v}{\partial t} + yu = -\frac{\partial \Phi}{\partial y} - uv \quad (2)$$

$$\frac{\partial \Phi}{\partial t} + D + dD_b = -P_r - \mu \Phi \quad (3)$$

$$\frac{\partial q}{\partial t} + \bar{Q}D + \bar{Q}_b dD_b + u \frac{\partial \bar{Q}}{\partial x} + du_b \frac{\partial \bar{Q}_b}{\partial x} + v \frac{\partial \bar{Q}}{\partial y} + dv_b \frac{\partial \bar{Q}_b}{\partial y} = Ev - P_r \quad (4)$$

$$\frac{\partial u_b}{\partial t} - yv_b = -\frac{\partial \Phi}{\partial x} - E_k u_b \quad (5)$$

$$\frac{\partial v_b}{\partial t} + yu_b = -\frac{\partial \Phi}{\partial y} - E_k v_b \quad (6)$$

Equation (3) is the combined hydrostatic, continuity and thermodynamic equation. Equation (4) is the vertically integrated moisture equation. Equations (5) and (6) are momentum equations for the barotropic BL. u , v and Φ represent the free-tropospheric low-level zonal wind, meridional wind and geopotential, respectively. μ and ν are Newtonian cooling and Rayleigh friction coefficients. q is the column-integrated perturbation moisture and is essentially dominated by the moisture from surface up to mid-troposphere. P_r and Ev are precipitation and evaporation, respectively. \bar{Q} and \bar{Q}_b are normalized basic-state specific humidity at the lower tropospheric layer and the BL, respectively (see Table 1 for definition of the parameters),

Table 1 Parameters and their standard values used in the experiments

| Parameter | Description | Typical value utilized here |
|-------------|---|--|
| Δp | Half-pressure depth of the free atmosphere | 400 hPa |
| P_s | Pressure at the surface | 1000 hPa |
| P_e | Pressure at boundary layer top | 900 hPa |
| P_u | Pressure at upper boundary | 100 hPa |
| P_2 | Pressure at level 2 | 500 hPa |
| C_0 | Dry gravity wave speed of the baroclinic mode | 50 m s ⁻¹ |
| ν^* | Dimensional Rayleigh friction | (16 day) ⁻¹ |
| μ^* | Dimensional Newtonian cooling coefficient | (8 day) ⁻¹ |
| τ^* | Convective adjustment time | 2.0 h |
| α | Moisture reference coefficient | 0.1 |
| E_k^* | Dimensional Ekman number in the boundary layer | 2.3 × 10 ⁻⁵ s ⁻¹ |
| m | Density scale height/water vapor density scale height | 3.45 |
| SST | Sea surface temperature | 29.0 °C |
| b | Precipitation efficiency coefficient | 0.88 |
| d | $d = (p_s - p_e)/\Delta p$ Nondimensional boundary layer depth | 0.25 |
| \bar{Q} | $\bar{q}_3/(d_0)$ | 0.98 |
| \bar{Q}_b | $\bar{q}_e/(d_0)$ | 1.98 |
| d_0 | $d_0 = \frac{2p_2 C_p C_0^2}{\Delta p R L_c}$ | 0.008 |

both are controlled by the underlying sea surface temperature (SST) (Wang 1988b), the relation between them and the SST are given in Appendix 1. For homogeneous SST, the zonal and meridional moisture advection in Eq. (4) will vanish. D and D_b are the lower-tropospheric and BL divergence, respectively. u_b and v_b are BL barotropic winds, and E_k is the friction coefficient in the BL. d is the nondimensional BL depth. The definition and standard values for the model parameters are listed in Table 1.

3.3 Parameterization of precipitation heating

Two simple schemes are examined in the present study.

- (a) Simplified Kuo scheme, in which the moisture tendency is neglected in (4), and precipitation is balanced by horizontal moisture convergence and surface evaporation:

$$P_r = bH(E_v - (\bar{Q}D + \bar{Q}_b dD_b)) \tag{7}$$

where b is precipitation efficiency coefficient. $H(x)$ is a Heaviside function, which represents the positive-only precipitation (Justification is given in Appendix 2).

- (b) Simplified B–M scheme, in which the moisture tendency is retained in Eq. (4), and precipitation heating must be parameterized in order to close the governing equations. The B–M (Betts and Miller 1986; Betts 1986) scheme relaxes temperature and humidity back

to a reference profile when some convective criteria are met. Following Frierson et al. (2004), the humidity is relaxed back to a reference value \tilde{q} , at which precipitation occurs (see Appendix 2):

$$P_r = \frac{1}{\tau}H(q - \tilde{q}(T)) \tag{8}$$

where τ is a convective adjustment time scale, $\tilde{q}(T)$ is a function of temperature. The $q - \tilde{q}(T)$ could be considered as a mimic of CAPE in this model (Frierson et al. 2004). Therefore, Eq. (8) represents relaxation of CAPE over a finite time scale τ , keeping CAPE in a quasi-equilibrium state. For simplicity, $\tilde{q}(T)$ is assumed to be proportional to free troposphere temperature, which in this model is related to low-level geopotential, hence, $\tilde{q}(T) = \alpha\Phi$, where α is a constant coefficient. Thus, precipitation has the form:

$$P_r = \frac{1}{\tau}H[(q + \alpha\Phi)] \tag{9}$$

The τ measures the time over which convection releases CAPE and relaxes moisture back to its reference state. A small τ implies an intense cumulus activity and a rapid atmospheric adjustment toward the quasi-equilibrium reference state; a large τ means that thermodynamics is less tightly constrained (Neelin and Yu 1994). Betts and Miller (1986) suggested an appropriate value of τ being about two hours. The other parameter, α , is related to the intensity of CAPE. With

a small α , CAPE is large and precipitation is intensive. When α is combined with convective adjustment time, the coefficient τ/α could be considered as buoyancy relaxation time (Fuchs and Raymond 2002).

4 Realistic simulation of the MJO characteristics

Figure 3 presents the life cycle of the simulated MJO on an aqua-planet with a uniform SST of 29.0 °C by using simplified Kuo and B–M schemes, respectively. For simplicity the evaporation was neglected, because it is not an essential driver and without background flow it cannot be adequately described. In the presence of the BL dynamics, the two simulations reproduced the following common features: (a) a planetary (zonal) scale circulation system, (b) a coupled Kelvin–Rossby wave (horizontal) structure interacting and coupling with precipitation heating, (c) the BL low pressure and moisture convergence that lead the major convective precipitation region, and (d) eastward movement. Major difference is the propagation speed: 4.7 m/s in B–M simulation and 14.9 m/s in Kuo simulation. Here, we first discuss the common features simulated by the B–M scheme with moisture feedback.

The planetary (zonal) scale of the model MJO is further analyzed in Fig. 4a, b. The model MJO structure is primarily made of the zonal wave 1–4 (Fig. 4a), consistent with observed wavenumber domain of MJO (Wheeler and Hendon 2004; Jiang et al. 2015). Obviously, the wavenumber one component has the largest contribution (Fig. 4b). If we use an initial Kelvin wave low with different zonal scales, the solutions will converge to almost the same pattern with a planetary zonal scale after a few days' integration. Thus, the MJO solutions have preferred planetary zonal scales.

The low-level geopotential and wind fields simulated by B–M scheme (Fig. 5a) display a coupled Kelvin–Rossby wave pattern, resembling closely to the observed structure (Fig. 1b). Note that, as shown in Fig. 5b, the vorticity and stream function fields associated with the coupled Kelvin–Rossby wave structure shows a “quadrupole vortex” structure as mentioned in some literature (Kiladis et al. 2005; Zhang 2005; Majda and Stechmann 2009). The left (rear) cyclonic pair is the Rossby wave response to the heating, while the east (front) anticyclonic pair arises from the meridional shear vorticity of the equatorial easterlies associated with the Kelvin wave component.

Figure 5a also shows that the BL low pressure and moisture convergence are located under and to the east of the major convection center. This structural difference between the BL and free troposphere is the 1 and ½ layer model view of the observed backward tiled vertical structure in the vertical velocity and moisture fields. The vertical tilt of moisture field is mainly contributed by the BL frictional

convergence (FC) to the east of the convective heating. The vertical tilts of the moisture and vertical velocity fields in this model can only be resolved by BL dynamics as the free atmosphere is described by the lowest baroclinic mode. But there may exist other processes that contribute to lower-tropospheric moisture increase beside the BL convergence. The current model result suggests it is important to identify new mechanism that causes moisture increase in the lower troposphere. Also note that the BL convergence pattern may be a possible explanation of the swallowtail precipitation pattern as described by Zhang and Ling (2012).

Under homogeneous SST the precipitation anomaly grows with a constant rate (Fig. 3b). It is interesting to examine how the precipitation intensity evolves in a spatially varying background SST field. For this purpose, an idealized “warm pool” SST configuration is designed (Fig. 6a). With such a SST or basic state moisture setting, the simulated MJO precipitation moves eastward from 60°E to 170°E with a speed about 5 m/s. Interestingly, the simulated MJO is not a neutral mode or monotonic growing/decaying mode: its amplitude is modulated by the background SST. Precipitation anomaly amplifies over the warm ocean with the strongest precipitation nearly coinciding with the highest SSTs. The precipitation anomaly decays quickly near the dateline as the westward background SST gradients produces negative moisture advection by the MJO easterly in front of the precipitation, which tends to kill the convection.

There are two fundamental processes that interact with convective heating and support the MJO-like mode, one is the BL FC feedback and the other is moisture feedback. In the following two sections we will identify their different roles in MJO dynamics.

5 Important roles of the moisture feedback and mechanism of slow propagation

5.1 Impacts of moisture feedback

The moisture feedback effects can be readily identified by comparison of the simulations with Kuo and B–M schemes because in Kuo scheme the moisture feedback does not exist. Comparison of Fig. 3a, b reveals two salient effects of the moisture feedback with B–M scheme. First, the moisture feedback can substantially slow down the eastward propagation. For given SST = 29 °C, the propagation speed in the B–M simulation (about 5 m/s) is only one-third of that in Kuo simulation (about 15 m/s) (Fig. 3). Second, the moisture feedback can significantly change the horizontal structure of the MJO mode. This can be seen from Fig. 7 that compares the horizontal structures of the MJO modes simulated by B–M scheme and Kuo scheme. There are

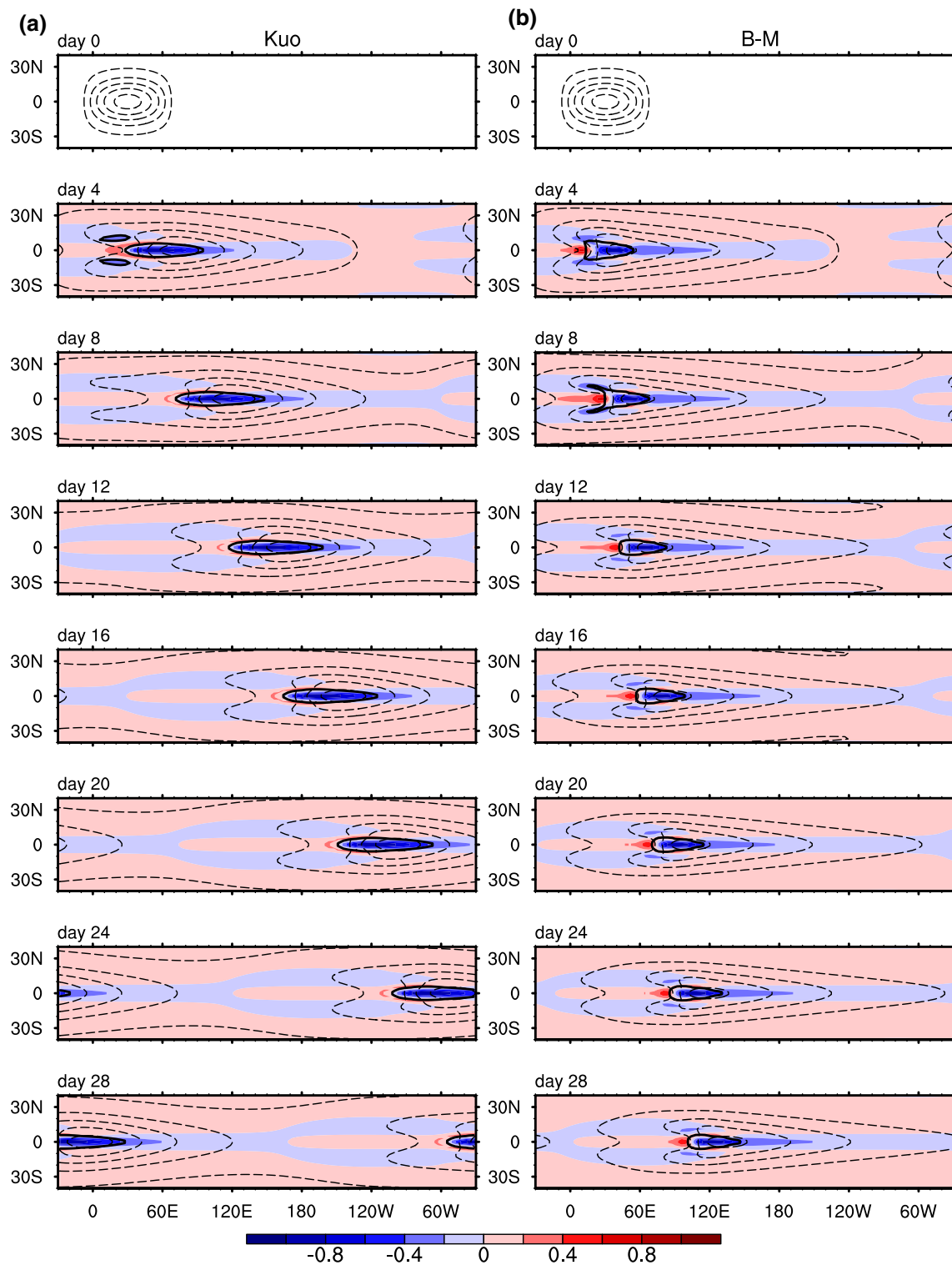


Fig. 3 Evolution and propagation of MJO modes simulated with simplified (a) Kuo- and (b) B–M cumulus parameterization. Shown are sequential maps of boundary layer divergence (*color shading*), lower troposphere geopotential height (*dashed contours*) and precipitation (*solid contour*). All fields are normalized by their respective maxima (*absolute values*) at each panel because the simulated MJO-

like mode grows exponentially. The *dash contours* start from -0.9 , and increases with interval of 0.2 . The *solid black contour outlines* the precipitation region where the normalized precipitation is over 0.1 . The basic state SST is uniform $29.0\text{ }^{\circ}\text{C}$. The initial perturbations are a “pure” dry Kelvin wave low pressure centered on the equator and 60°E and spanned 80° in longitude

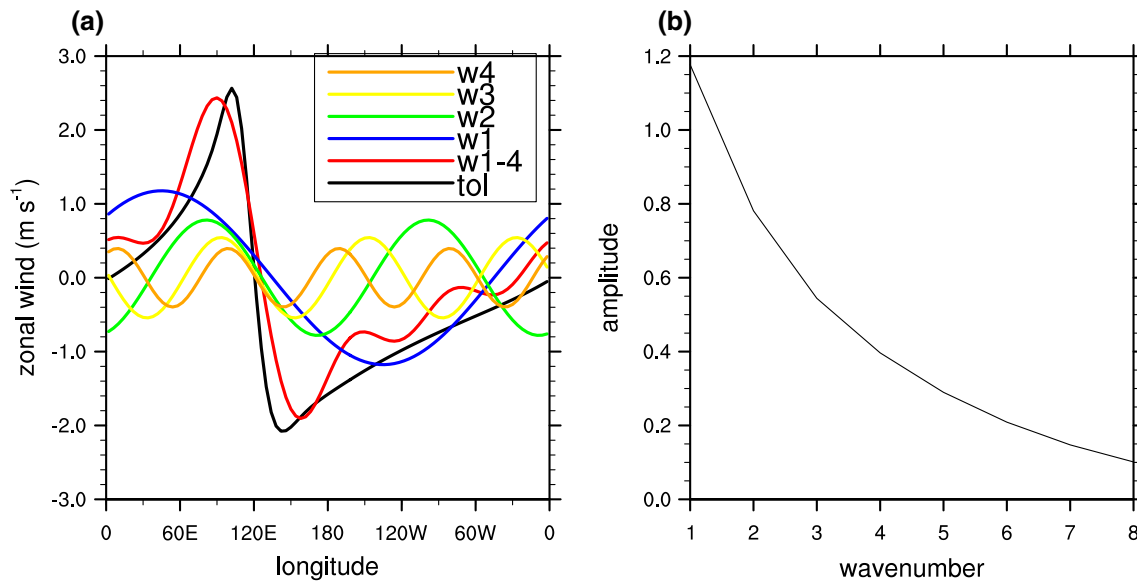


Fig. 4 **a** Planetary zonal scale of the MJO mode shown by the equatorial zonal wind (m/s) at day 20 in the B–M simulation (*black line*). The *red line* shows the approximate zonal wind made by the

first four wavenumbers. Other *lines* show the first four wavenumber components, respectively; **b** amplitude of each wavenumber (x-axis) obtained by Fourier analysis

three notable structural differences that indicate the effects of moisture feedback on simulated MJO structures.

First, the moisture feedback in B–M simulation makes the horizontal circulation shape more close to the Gill (1980) pattern (Fig. 7). The shape of circulation can be measured by a “shape” parameter, which is defined by the ratio of the zonal extent of the equatorial “Kelvin” easterly (below -0.2 in normalized value) versus “Rossby” westerly (above 0.2 in normalized value) averaged between 5°S and 5°N . In the Gill (1980) model, the circulation pattern, in response to a given heat source, has a shape parameter of 3.0. The shape parameter is roughly 2.4 in the B–M simulation but it is about 1.4 in the Kuo simulation. This shape parameter in B–M simulation is close to observation (about 2.1).

Second, the moisture feedback in the B–M simulation enhances the relative intensity of the Rossby wave (vs. Kelvin wave) component. Since the equatorial westerlies (easterlies) are primarily contributed by equatorial Rossby (Kelvin) waves, the Rossby wave intensity can be measured by a “westerly intensity” index, which is defined by the ratio of the equatorial maximum westerly speed U_{max} versus the maximum easterly speed $abs(U_{min})$. The westerly intensity index is 0.58 in Kuo simulation while it is 1.16 in the B–M simulation.

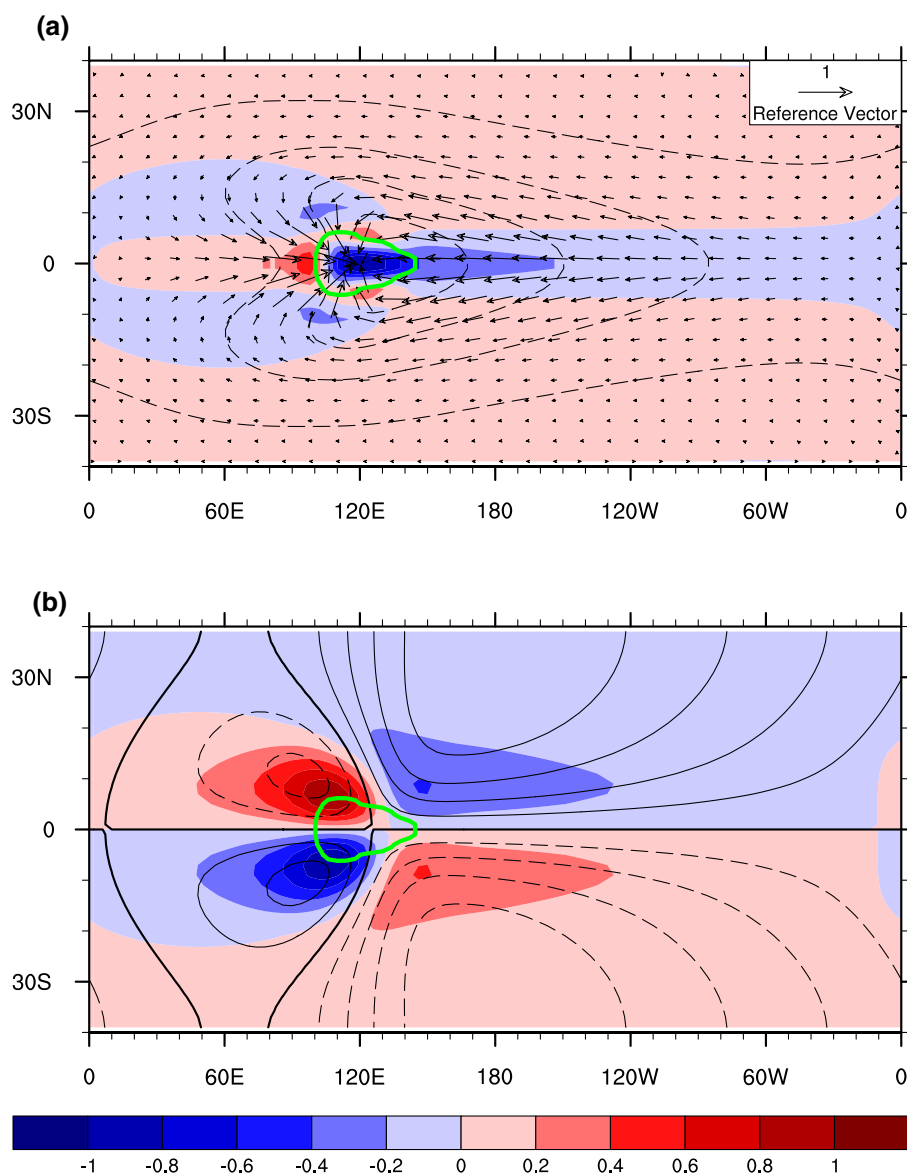
Third, the meridional extent of the circulation is smaller in the B–M simulation. This tighter equatorial trapping is a consequence of slower eastward propagation. The meridional trapping scale is determined by the equatorial Rossby Radius of Deformation, an intrinsic length scale

in equatorial dynamics, which is proportional to the wave propagation speed. Since the moisture feedback reduces the propagation speed of convectively coupled MJO mode, the “effective” Rossby Radius of Deformation also decreases.

Why does the moisture feedback in the B–M simulation substantially slow down the eastward propagation of the MJO mode? Surprisingly, we found that the MJO eastward propagation speed decreases when the Rossby wave component is enhanced. This inverse relation is shown in Fig. 8 where propagation speed is controlled by the background SST. Note that the propagation speeds for both the Kuo- and B–M simulations are inversely related to the relative intensity of the Rossby wave component. We therefore suggest that the enhanced Rossby wave component can substantially slow down eastward propagation of the MJO mode because the Rossby wave component induced by β -effect tends to move westward. The theoretical result here finds support from a previous aqua-planet numerical study, which shows that when Rossby wave component becomes weak, the eastward propagation becomes faster (Kang et al. 2013). The finding here is also consistent with the GCM simulation results in Fig. 1, where the poor MJO shows a much stronger Rossby wave component than the Kelvin wave component.

How does the B–M scheme enhance the Rossby wave component? We found that the B–M scheme produces a stronger coupling of the Rossby wave and convective heating than the Kuo scheme. This is evidenced by the fact that about 50% of the precipitation area coincides with Rossby westerly in the B–M simulation, while this ratio is only

Fig. 5 Horizontal structure of the simulated MJO mode at day 20 by using B–M scheme. **a** BL divergence (*shading*), low-level geopotential height (*contour*) and wind (*vector*). **b** Vorticity (*shading*) and stream function (*contour*). The wind vectors are normalized by the maximum wind speed. Other fields are normalized by their respective maxima (*absolute values*). The contour interval is 0.2. The *thin solid (dashed) contours* indicate positive (negative) values. The *dash contour* in (a) starts from -0.8 . The *thick black solid contour* in (b) denotes the zero contour. The *green solid contour* outlines the region where the normalized precipitation is over 0.1



about 30% in the Kuo simulation (Fig. 7). This stronger coupling is also evidenced by the fact that the precipitation center and the maximum Rossby westerly are closer in the B–M simulation than in the Kuo simulation. Thus, the moisture feedback in the B–M scheme couples more tightly the convection and Rossby waves, resulting in an enhanced Rossby wave component.

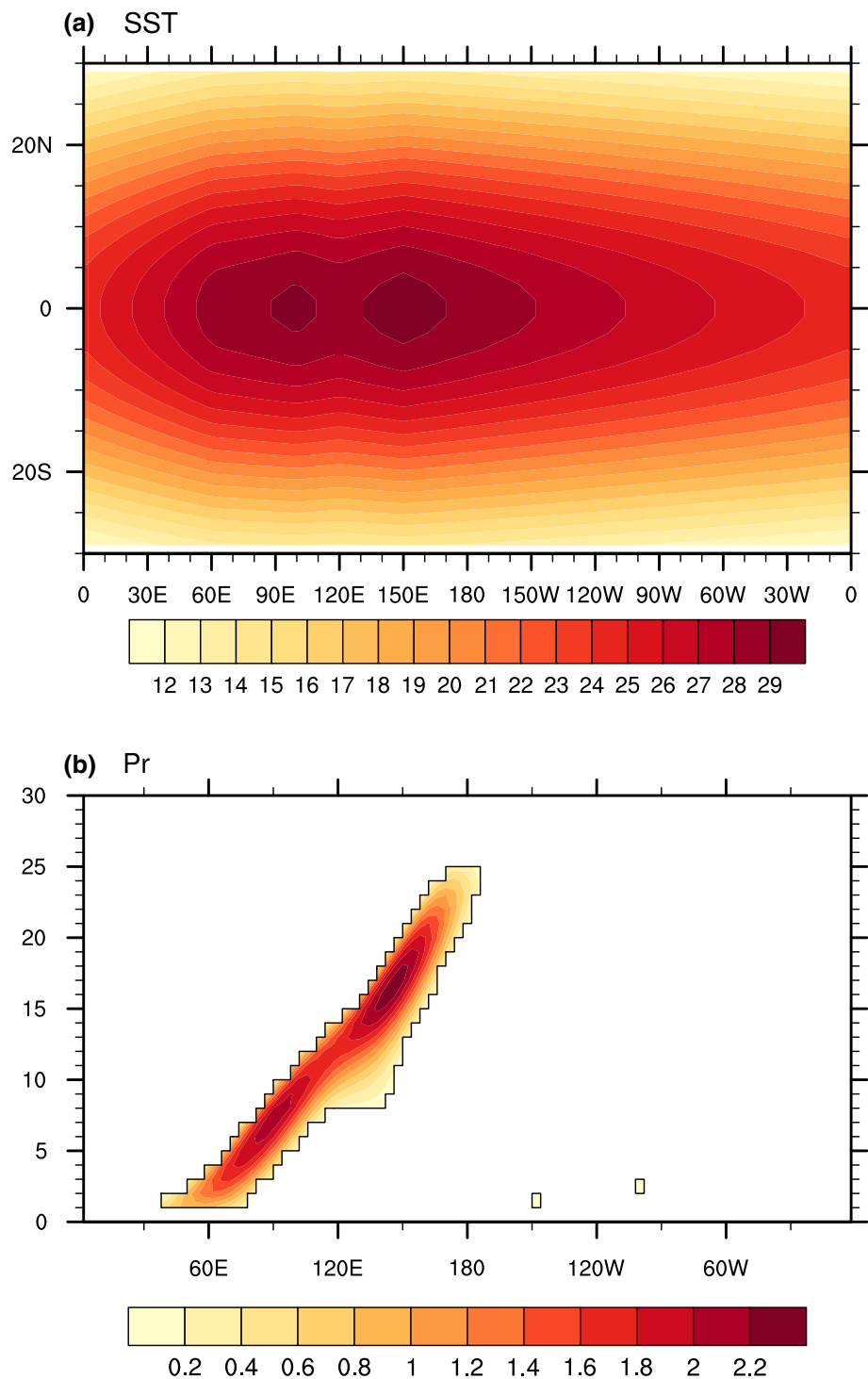
In sum, compared with the Kuo simulation, the moisture feedback in the B–M scheme can couple more tightly the Rossby waves and convection, thereby (a) enhance the Rossby wave component and substantially slow down eastward propagation of the MJO mode, (b) make the horizontal structure of the MJO mode more close to observed MJO structure, and (c) reduce the meridional extent of the MJO circulation due to the slow eastward propagation. Note that the effects of moisture feedback may depend on the

cumulus parameterization scheme. The effects discussed here is associated with the simplified B–M scheme.

5.2 Mechanisms for slow eastward propagation of MJO

Slow eastward propagation (about 5 m/s) in the eastern hemisphere is critical to explain the 30–60-day periodicity of MJO. What controls MJO propagation speed in general? In this subsection, we show that the slow eastward propagation is primarily attributed to (a) warm sea surface temperature (SST), which promotes convective heating that reduces static stability, (b) the coupling of Kelvin and Rossby waves, and (c) the moisture feedback in the B–M parameterization. To understand the effects of factors (a) and (b), it is convenient to examine the combined

Fig. 6 MJO propagation in varying background SST ($^{\circ}\text{C}$) simulated with B–M scheme. **a** Idealized Indo-Pacific warm pool SST configuration. **b** Time-longitude diagram of simulated precipitation rate (mm/day) along the equator. The initial perturbation is a “pure” dry Kelvin wave low pressure centered on the equator and 60°E and spanned 80° in longitude. The amplitude of the initial Kelvin wave geopotential height is 4 m. The zonal and meridional moisture advection were included. The Newtonian cooling and Rayleigh friction are both set to $(10 \text{ day})^{-1}$



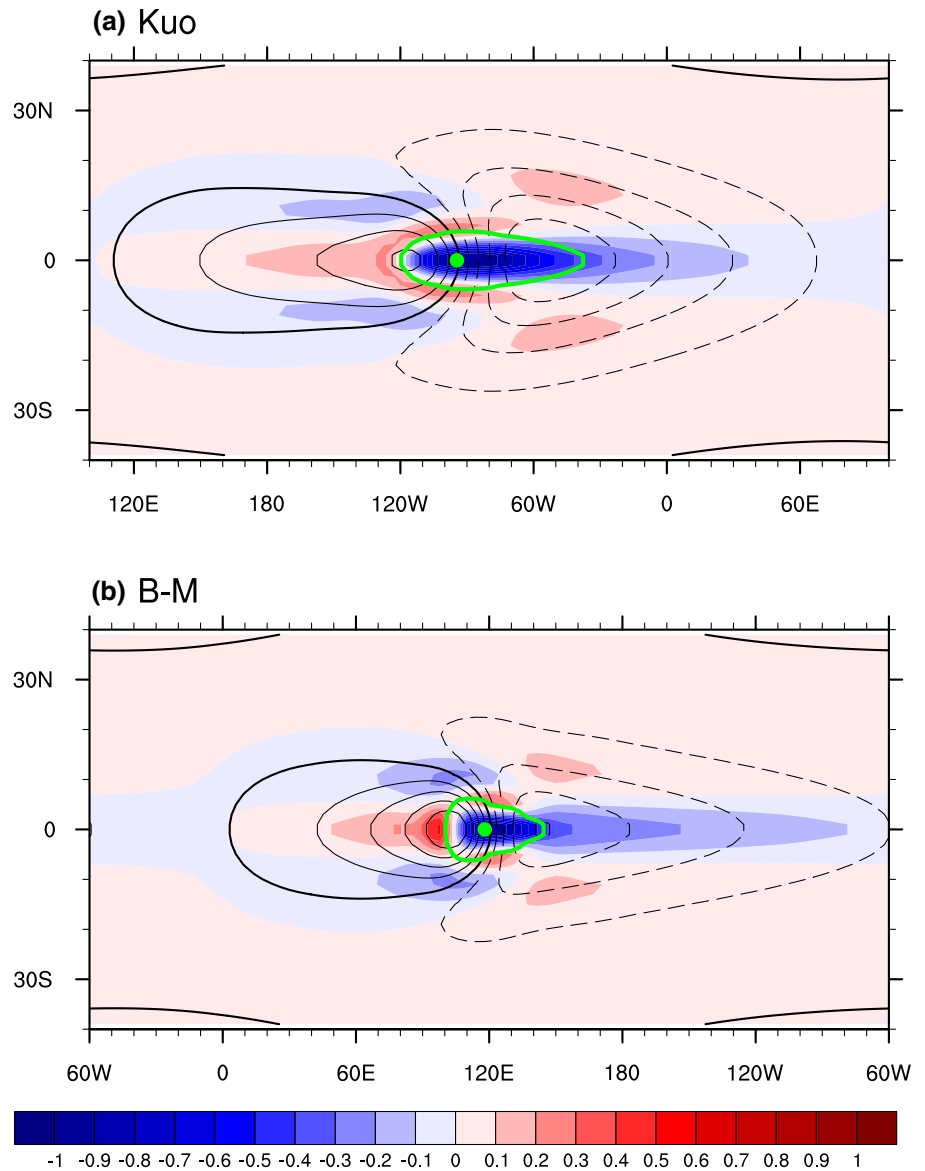
dimensional thermodynamic equation and moisture equation without BL and moisture tendency:

$$\frac{\partial \Phi}{\partial t} + C_0^2(1 - \bar{q}_3/q_c)\nabla \cdot \vec{v} = 0 \quad (10)$$

where C_0 is the dry Kelvin wave or gravity wave speed, which is determined by the dry static stability; q_c is

a scaling constant; the quantity $C_0^2(1 - \bar{q}_3/q_c)$ represents the effective static stability, which is the reduced static stability due to the precipitation heating. Thus, $C = C_0\sqrt{(1 - \bar{q}_3/q_c)}$ is the phase speed of convectively coupled Kelvin wave. When SST increases, the (\bar{q}_3) increase accordingly, thus moist Kelvin wave phase speed decreases. As shown in Fig. 9, given all model parameters

Fig. 7 Comparison of horizontal structures of the MJO modes simulated by (a) Kuo and (b) B–M scheme at day 20. All fields are normalized by their respective maxima (*absolute values*) at each panel. The *green lines* outline the region where the normalized precipitation rate is larger than 0.1. The *thin solid (dashed) contours* indicate positive (negative) low-level zonal wind speed with a contour interval of 0.2. The *thick black solid line* denotes the zero contours. The *green dot* in each panel represents the location of maximum precipitation



being the same (Table 1), the dry Kelvin (gravity) wave speed is 50 m/s, whereas the convectively coupled Kelvin wave (moist-K) speed decreases with increasing SST with a value of 19 m/s for SST = 29 °C. The MJO eastward propagating speed is further slowed down by the coupling of Kelvin and Rossby waves from 19 to 14.9 m/s when SST = 29 °C with the simplified Kuo scheme. This is because the Rossby wave component induced by β -effect tends to move westward. Finally, the moisture feedback can further significantly slow down the eastward propagation speed to about 5 m/s with simplified B–M scheme. The SST-dependence of propagation speed is consistent with

the observed slow propagation over the warm pool and fast propagation in the cold ocean in the western hemisphere (Knutson et al. 1986).

Note that an increase in SST would not only increase water vapor, which tends to reduce convectively coupled wave speed, but also increase the atmospheric static stability that tends to increase convectively coupled wave speed. Therefore, the model static stability parameter should not be fixed, rather it should increase with SST accordingly. The increasing static stability can accelerate convectively coupled Kelvin waves in warm climate, potentially consistent with the result of Kuang (2008).

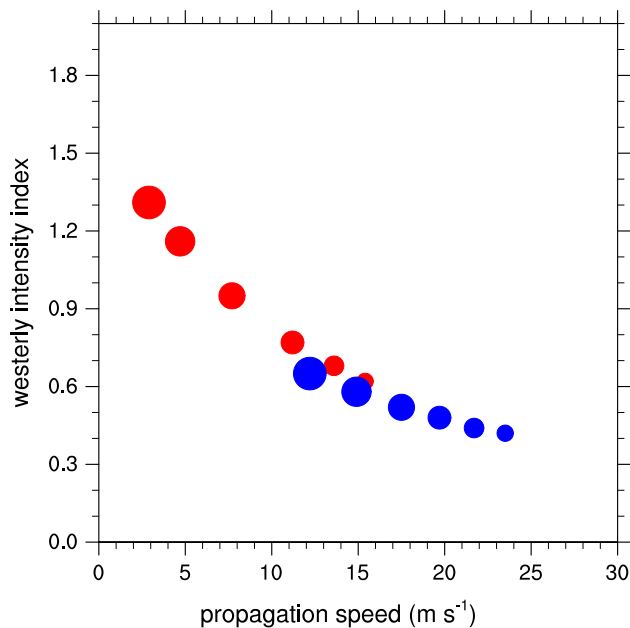


Fig. 8 Propagation speed as a function of Westerly intensity index in the B–M simulation (*red filled cycle*) and Kuo simulation (*blue filled cycle*). The Westerly intensity index is defined as the ratio of the maximum MJO westerly versus the maximum MJO easterly speed averaged between 5°S and 5°N. The sizes of the cycles are proportional to the SST, which varies from 27.0 to 29.5 °C, with a 0.5 °C interval

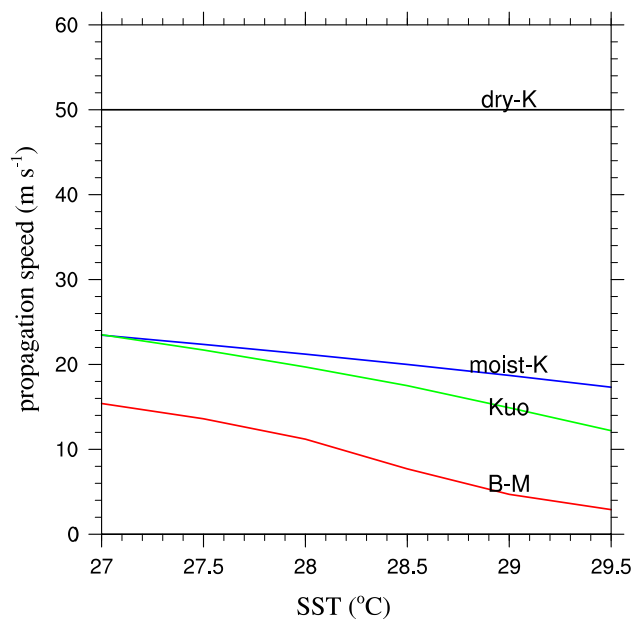


Fig. 9 Eastward propagation speed as function of SST for dry Kelvin wave (Dry-K), moist Kelvin wave (moist-K), coupled Kelvin–Rossby waves in the Kuo simulation (Kuo) and in the B–M simulation (B–M)

6 Critical roles of the FC feedback in MJO structure and eastward propagation

What process is responsible for the coupling of the Kelvin and Rossby waves? Could the moisture feedback process couple the Kelvin and Rossby waves together and propagate eastward? To address this question, we use a simplified version of the model with the B–M scheme and moisture feedback but *without BL dynamics* (by setting the BL depth d to zero). The model configuration is the same as that used in Fig. 3; thereby the results can be readily compared with those obtained by B–M scheme with the BL dynamics (Fig. 3b). The model without BL can isolate the role of the moisture feedback, while comparison of the simulation results with and without BL can identify the role of the BL FC feedback.

Figure 10 shows that in both experiments, the initial dry Kelvin wave low pressure induces precipitation, which further excites a coupled Kelvin–Rossby system, as is shown in day 2. The evolution, however, diverges after a 2-day initial adjustment process. Without the BL dynamics, the Kelvin and Rossby waves are decoupled after day 2: The Rossby wave moves westward and the Kelvin wave moves eastward. Their separate propagation speeds are the same as predicted by the equatorial Kelvin and long Rossby wave theory. Therefore, the moisture feedback in the B–M parameterization could not generate the MJO-like mode without invoking the BL dynamics.

One of the central questions for MJO theory to be addressed is how could the eastward propagating Kelvin wave and westward propagating Rossby waves be coupled together with convection and select eastward propagation? The answer is in the BL dynamics. The Rossby wave-induced BL convergence exhibits not only off-equatorial maximum coinciding with Rossby wave lows but also an equatorial maximum convergence to the east of the Rossby wave lows; on the other hand, the Kelvin wave-induced BL convergence displays a trapped equatorial maximum that coincides with Kelvin wave low pressure and easterly phase (Wang and Rui 1990a). Therefore, when convective heating excites Rossby wave westerly to its west and Kelvin wave easterly to its east, the Kelvin and Rossby waves would produce a unified BL moisture convergence field that coincides and leads the major convective heating (see Fig. 5a). As a result, the frictional organization of convective heating can couple the Kelvin and Rossby waves together. The BL moisture convergence can also accumulate moist static energy and increase convective instability to the east of the major convection (Hsu and Li 2012), leading to eastward propagation of the MJO.

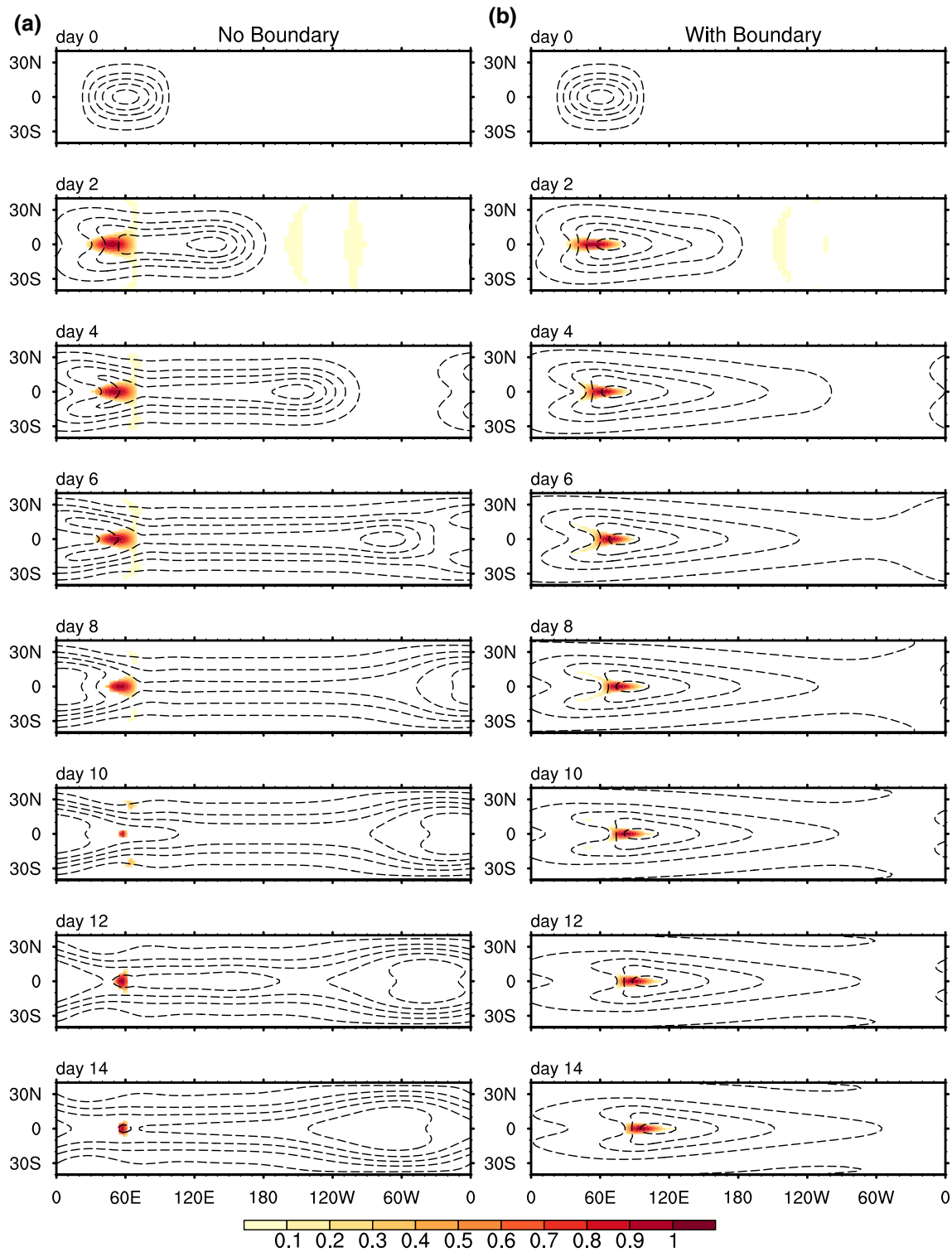


Fig. 10 Comparison of the evolution/propagation of the simulated MJO modes in the B–M simulation and (a) without and (b) with the boundary layer dynamics. Shown are sequential maps of precipitation rate (color shading) and lower troposphere geopotential height (con-

tours). All fields are normalized by their respective maxima (absolute values) at each panel. The contours start from -0.9 with an interval 0.2 . The basic state SST is uniform $29.0\text{ }^{\circ}\text{C}$

7 Conclusion and discussion

A general theoretical model for understanding essential dynamics of the MJO is advanced. The model physics include free tropospheric low-frequency equatorial wave dynamics, BL dynamics, full thermodynamics with simplified Betts–Miller (B–M) convective parameterization schemes, and a full moisture conservation equation. The model describes the moisture feedback and trio-interaction among convective heating, low-frequency Kelvin and Rossby waves and the BL friction convergence (FC) (Fig. 2). A simplified version of the current model, in which a linear heating, steady BL, and highly truncated meridional structure of the motion were assumed and a complementary eigenvalue analysis of linear instability of the ‘dynamic’ moisture mode was carried out (Liu and Wang 2016). They explored the effects of BL process and the moisture feedback on the MJO by studying an eigenvalue problem, focusing on analytical solution of the linear instability of the ‘dynamic’ moisture mode. The model here is more general, allowing for considering realistic basic state SST, transient BL, and nonlinear heating etc., simulating more realistic evolution, propagation and structure, and elaborating mechanisms by which moisture feedback slowing down the eastward propagation and the linkage between propagation and horizontal structure. This general model framework can accommodate different cumulus parameterization schemes, such as Majda and Stechmann (2009) parameterization, in which precipitation tendency is linked to the moisture anomaly. The general model framework can readily include other processes that are deemed to have important impacts on MJO’s evolution, such as eddy momentum, moisture and heat transfer as well as effects of advection of the moisture. The present model can also be extended to a multi-layer model to incorporate multi-layer cloud precipitation effects and explore stratiform cloud–wave interaction and radiation–cloud interaction.

7.1 Conclusion

The general model with B–M scheme yields a frictionally coupled dynamic moisture mode, which reproduces the following essential characteristics of the observed MJO (Figs. 3, 4, 5, 6): (1) a coupled Kelvin–Rossby wave structure, (2) slow eastward propagation (~ 5 m/s) over warm pool, (3) planetary (zonal) scale circulation, (4) a vertical structure in which BL moisture convergence leads major convection, and (5) grow/decay over warm/cold SST regions.

The FC feedback provides a mechanism that couples the Kelvin wave and Rossby wave together along with convective heating, and selects eastward propagation. Without FC feedback, the Kelvin and Rossby waves are decoupled,

and there is no growing mode (Fig. 10). Therefore, the FC feedback acts like an engine that drives the wave dynamic feedback and moisture feedback to generate the unstable dynamic moisture mode.

The moisture feedback in a simplified Betts–Miller scheme can enhance the relative intensity of Rossby wave response in the MJO structure (Fig. 7). Interestingly, the eastward propagation speed decreases when the relative intensity of the Rossby wave component increases (Fig. 8). Thus, the moisture feedback can substantially reduce the eastward propagation speed to a realistic value (Fig. 9). In addition, the moisture feedback makes the convection and Rossby wave couple more tightly, resulting in a more realistic horizontal structure.

Our novel finding on the inverse relationship between eastward propagation speed and the relative intensity of the Rossby wave component seems to be consistent with the difference between the models’ simulated good and poor MJOs (Fig. 1, the westerly intensity indices along equator are about 0.8 and 2.4 for the good and poor MJO), but needs to be further verified by observations and model results.

7.2 The sensitivity of solutions to model parameters

The model solutions vary with the model parameters. The most sensitive parameters are the BL Ekman number and the convective adjustment time in the B–M scheme. The Ekman number E_k (Wang 1988b), $E_k = \rho_e g A_z / ((p_s - p_e) h \ln(h/z_0))$, is determined by the turbulence viscosity coefficient A_z (with typical value $10 \text{ m}^2 \text{ s}^{-1}$), the surface roughness z_0 (with typical value 0.01 m), the height of the surface layer h (with typical value 60 m), as well as the BL depth $(p_s - p_e)$, or nondimensional BL depth d (typical value is 0.25). Thus, the typical value of E_k used in our study is $2.3 \times 10^{-5} \text{ s}^{-1}$, which corresponds to BL damping time scale of approximately 0.5 day. This value is as the same as that used in Mori and Watanabe (2008). This value is also used to compensate the neglected effects of complex nonlinear processes.

Table 2 shows the sensitivity of the B–M simulations to the BL friction E_k . As the BL friction decreases (smaller E_k), the BL winds and thus the BL convergence increases. The enhanced BL convergence has two effects on the simulated MJO-like modes. First, it enhances moisture feedback, which results in enhanced Rossby wave component, as manifested by the westerly intensity index (Table 2). This slows down eastward propagation. Second, the stronger BL moisture convergence results in stronger instability of the simulated MJO-like mode.

Table 3 shows the model sensitivity to the convective adjustment time τ . First, for a longer τ , the relative strength of the Rossby wave component is weaker, thereby the eastward propagation is faster. The reason is that a longer τ means slower atmospheric adjustment toward the

Table 2 Sensitivity of B–M simulation to Ekman number E_k for the B–M simulation, assuming $d = 0.25$ and SST = 29.0 °C

| E_k percentage change | 180 (%) | 160 (%) | 140 (%) | 120 (%) | 100 (%) | 80 (%) | 60 (%) | 40 (%) | 20 (%) |
|--------------------------|---------|---------|---------|---------|---------|--------|--------|--------|--------|
| Damping time (day) | 0.28 | 0.31 | 0.36 | 0.42 | 0.5 | 0.63 | 0.83 | 1.25 | 2.5 |
| Propagation speed (m/s) | 7.8 | 7.4 | 6.7 | 5.9 | 4.7 | 3.1 | 1.5 | −0.37 | −2.25 |
| Westerly Intensity Index | 0.80 | 0.89 | 0.96 | 1.05 | 1.16 | 1.30 | 1.45 | 1.60 | 1.67 |
| Growth rate (1/day) | 0.06 | 0.10 | 0.13 | 0.17 | 0.21 | 0.27 | 0.35 | 0.51 | 0.84 |

The growth rate is defined as the exponential growth rate of the total eddy energy averaged over the whole domain (averaged from day 5 to day 25)

Table 3 Sensitivity of B–M simulation to convective time scale τ , assuming $d = 0.25$ and SST = 29.0 °C

| Convective time scale (h) | 1 | 2 | 4 | 6 | 8 |
|---------------------------|------|------|------|------|-------|
| Propagation speed (m/s) | 3.0 | 4.7 | 6.9 | 8.8 | 9.1 |
| Growth rate (1/day) | 0.38 | 0.21 | 0.08 | 0.02 | −0.00 |
| Westerly Intensity Index | 1.32 | 1.16 | 0.92 | 0.81 | 0.78 |

quasi-equilibrium reference state. Thus, the role of moisture feedback in enhancing Rossby wave would be weaker. Second, a longer τ means reduced precipitation intensity, which leads to weaker instability.

Our experiment results (not shown) indicate that the planetary zonal scale of the MJO mode in this model is not sensitive to the Ekman parameter and the convective adjustment time scale. This result is different to Pritchard and Yang (2016) who showed the zonal scale change with SST. A possible reason is that the present model does not include the mean circulation. In the SPCAM model they used, the Hadley circulation is enhanced with SST, but is missing when SST is 25 °C and reverses its sign below 25 °C (downward motion over equator). The dramatic change of the mean circulation may cause the differences in the zonal scale of their MJO-like mode. However, these changes could not be represented in our model.

7.3 Implications

The results of this study suggest that MJO propagation is sensitive to the cumulus parameterization schemes because different schemes may produce different structures of the MJO and propagation speed is related to the horizontal structure. Even within the chosen B–M scheme, the eastward propagation speed depends on sensitive parameters such as the convective adjustment time τ . This may explain why a variety of MJO behaviors have been produced in GCMs and why tuning parameters or change of cumulus parameterization can effectively improve the MJO simulation.

The model here does not have shallow convection due to the simple vertical structure of the model. But the BL moisture convergence-induced heating is added to the mid-level,

which is located to the east of the major convection center. In this sense, the shallow convection effect is represented in the model by the “deep’ convection to the east of the major convection. In GCMs, the BL FC always exists. However, the way by which BL convergence interacts with shallow convection in different GCM may differ and this interaction could significantly affect MJO behavior. The BL convergence can enhance shallow convective heating and upward transport of moisture that further feeds back to BL moisture convergence. This positive feedback could amplify the effects of FC feedback. This implies that MJO simulation may be sensitive to shallow cumulus parameterization schemes in GCMs. This process should be taken into account in the numerical modeling of MJO with GCMs.

Acknowledgements This work has been supported by the NSF Award #AGS-1540783 and the Atmosphere–Ocean Research Center sponsored by the Nanjing University of Information Science and Technology and University of Hawaii. The authors thank Dr. Sun-Seon Lee for help with plotting Fig. 1 and anonymous reviewers for their constructive comments. This is the SEOST publication 9866, IPRC publication 1222 and ESMC publication 133.

Open Access This article is distributed under the terms of the Creative Commons Attribution 4.0 International License (<http://creativecommons.org/licenses/by/4.0/>), which permits unrestricted use, distribution, and reproduction in any medium, provided you give appropriate credit to the original author(s) and the source, provide a link to the Creative Commons license, and indicate if changes were made.

Appendix 1

Model description

Governing equations

The tropical motion can be described by the following primitive equations linearized about a rest atmosphere on an equatorial β -plane (Wang and Rui 1990a):

$$\frac{\partial u}{\partial t} - \beta yv = -\frac{\partial \Phi}{\partial x} - \nu u \quad (11)$$

$$\frac{\partial v}{\partial t} + \beta y u = -\frac{\partial \Phi}{\partial y} - \nu v \tag{12}$$

$$\frac{\partial T}{\partial t} - S_p \omega = \frac{1}{C_p} Q_c - \mu T \tag{13}$$

$$\frac{\partial u}{\partial t} + \frac{\partial v}{\partial y} + \frac{\partial \omega}{\partial p} = 0 \tag{14}$$

$$\frac{\partial \Phi}{\partial p} = -\frac{R}{p} T \tag{15}$$

$$\frac{\partial q}{\partial t} + \frac{1}{g} \int_{p_u}^{p_s} \nabla \cdot (\bar{q} \bar{V}) dp = E_v - P_r \tag{16}$$

In Eqs. (11–16), the dependent variables, u , v , ω , T , Φ and q , denote zonal wind, meridional wind, vertical pressure velocity, temperature, geopotential height and column-integrated water vapor; ν denotes Reighley friction and μ denotes a constant coefficient for Newtonian cooling; Q_c represent the condensational heating rate per unit mass; R and C_p are the gas constant of the air and the specific heat at constant pressure, respectively; E_v and P_r are the evaporation and precipitation rate; \bar{q} is the basic state of specific humidity; p_s and p_u are pressures at the lower and upper boundaries.

For a barotropic BL, the equations could be expressed as:

$$\frac{\partial u_b}{\partial t} - \beta y v_b = -\frac{\partial \Phi_e}{\partial x} - E_k u_b \tag{17}$$

$$\frac{\partial v_b}{\partial t} + \beta y u_b = -\frac{\partial \Phi_b}{\partial y} - E_k v_b \tag{18}$$

$$\omega_e = \left(\frac{\partial u_b}{\partial x} + \frac{\partial v_b}{\partial y} \right) (p_s - p_e) \tag{19}$$

where u_b and v_b are vertical averaged BL winds; Φ_e is the geopotential at the top of the BL; p_s and p_e are pressures at the surface and the top of the BL; ω_e is the vertical velocity at the top of the BL, and E_k is the friction coefficient in the BL.

2_{1/2} layer model

Writing Eqs. (11–15) in 2 and 1/2 layer model, and defining barotropic and baroclinic parts of the wind and geopotential height:

$$A_+ = \frac{1}{2}(A_1 + A_3) \tag{20}$$

$$A_- = \frac{1}{2}(A_3 - A_1) \tag{21}$$

where subscript + represents barotropic part and—represents baroclinic part, then the baroclinic mode could be obtained:

$$\frac{\partial u_-}{\partial t} - \beta y v_- = -\frac{\partial \Phi_-}{\partial x} - \nu u_- \tag{22}$$

$$\frac{\partial v_-}{\partial t} + \beta y u_- = -\frac{\partial \Phi_-}{\partial y} - \nu v_- \tag{23}$$

$$\left(\frac{\partial}{\partial t} + \mu \right) \Phi_- + C_0^2 = -\left(\frac{\partial u_-}{\partial x} + \frac{\partial v_-}{\partial y} \right) + \frac{C_0^2}{2\Delta p} (\omega_e + \omega_u) = \frac{R\Delta p}{2C_p p_2} (Q_2) \tag{24}$$

$$\omega_2 = \Delta p \left(\frac{\partial u_-}{\partial x} + \frac{\partial v_-}{\partial y} \right) + \frac{\omega_e + \omega_u}{2} \tag{25}$$

where $C_0 = (S_p \Delta p^2 R / (2p_2))^{1/2}$. ω_u is the vertical velocity at the top of the model, and is related to the barotropic mode by the relation:

$$\frac{\partial u_+}{\partial x} + \frac{\partial v_+}{\partial y} + \frac{\omega_e - \omega_u}{2\Delta p} = 0 \tag{26}$$

If we assume $\omega_u = \omega_e$, then the baroclinic mode is decoupled with the barotropic mode, and Eq. (24) reduces to:

$$\left(\frac{\partial}{\partial t} + \mu \right) \Phi_- + C_0^2 \left(\frac{\partial u_-}{\partial x} + \frac{\partial v_-}{\partial y} \right) + C_0^2 d \left(\frac{\partial u_b}{\partial x} + \frac{\partial v_b}{\partial y} \right) = -\frac{R\Delta p}{2C_p p_2} (Q_c) \tag{27}$$

where $d = \frac{p_s - p_e}{\Delta p}$.

Since the effects of the barotropic mode is small (Wang and Rui 1990a), we further assume that the barotropic mode vanishes, $A_+ = (A_3 + A_1)/2 = 0$. Thus, we have $A_3 = -A_1$ and $A_- = (A_3 - A_1)/2 = A_3$. In this case, the baroclinic mode represents the lower-level atmospheric variable, and the 2 and 1/2 model reduces to 1 and 1/2 model. For simplicity, we could drop the minus signs in Eqs. (22)–(23) and Eq. (27).

To describe interactive heating, the condensational heating rate Q_c in Eq. (27), is constrained by precipitation:

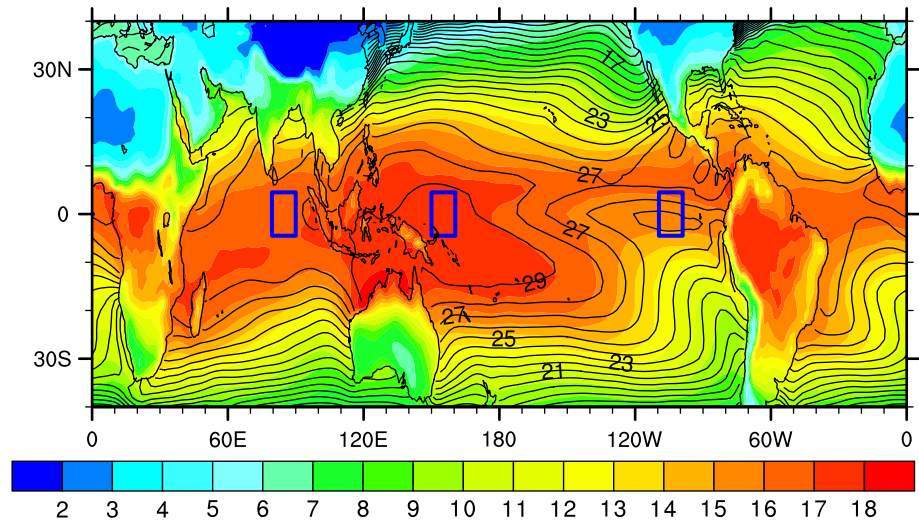
$$Q_c = \frac{g}{\Delta p} L_c H(Pr) \tag{28}$$

where $H(x)$ is a Heaviside function, which represents the positive-only precipitation.

The moisture Eq. (16) in 1 and 1/2 layer model can be expressed as:

$$\frac{\partial q}{\partial t} + \frac{1}{g} [\omega_2 (\bar{q}_3 - \bar{q}_1) + \omega_e (\bar{q}_e - \bar{q}_3)] + \frac{1}{g} \int_{p_u}^{p_s} (v \cdot \nabla \bar{q}) dp = E_v - P_r \tag{29}$$

Fig. 11 Climatological mean 1000 hPa specific humidity (*shading*) and sea surface temperature (SST, *contour*). The specific humidity is scaled by 10^{-3} . The three *box* locations represent Eastern Indian Ocean (EIO), Equatorial Western Pacific (EWP) and Equatorial Eastern Pacific (EEP) used in Fig. 12



If we neglect \bar{q}_1 , Eq. (29) can be written as:

$$\begin{aligned} \frac{\partial q}{\partial t} + \frac{\Delta p}{g} \bar{q}_3 \left(\frac{\partial u}{\partial x} + \frac{\partial v}{\partial y} \right) + \frac{\Delta p}{g} d\bar{q}_e \left(\frac{\partial u_b}{\partial x} + \frac{\partial v_b}{\partial y} \right) \\ + \frac{\Delta p}{g} u \frac{\partial \bar{q}_3}{\partial x} + \frac{\Delta p}{g} d\bar{q}_e u_b \frac{\partial \bar{q}_e}{\partial x} \\ + \frac{\Delta p}{g} v \frac{\partial \bar{q}_3}{\partial y} + \frac{\Delta p}{g} d\bar{q}_e v_b \frac{\partial \bar{q}_e}{\partial y} = E_v - P_r \end{aligned} \quad (30)$$

where the minus sign for the baroclinic mode has been dropped.

In summary, the Eqs. (17, 18), (22, 23), (27, 28) and (30) form a closed system if the precipitation and evaporation are parameterized in terms of existing variables.

The basic state

The basic state is a resting atmosphere on an aqua-planet. Figure 11 shows that over the oceans and on the timescale of a month or so, the surface specific humidity \bar{q}_s is well correlated with SST. Thus the basic state \bar{q}_s may be approximately computed from the following empirical formula established by (Wang 2012):

$$q_s(SST) = (0.94 \times SST(^{\circ}C) - 7.64) \times 10^{-3} \quad (31)$$

The vertical profile of the basic-state specific humidity is derived based on the observation that atmospheric absolute humidity over tropical ocean decays exponentially with a water vapor scale height H_1 (about 2.2 km) (Tomasi 1984). Thus, the basic state specific humidity can be expressed as a function of pressure (Wang 1988b):

$$\bar{q}(p) = \bar{q}_s \left(\frac{p}{p_s} \right)^{m-1} \quad (32)$$

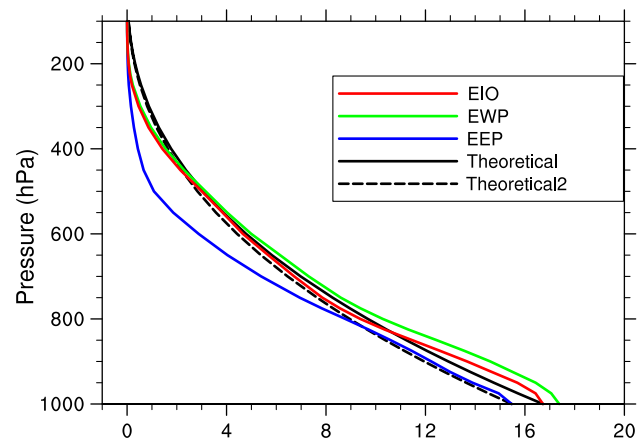


Fig. 12 Observed vertical profiles of specific humidity averaged over EIO, EWP and EEP (locations are shown in Fig. 12). The *black solid/dash curve* shows the vertical profile used as basic-state specific humidity in the unified model when the surface specific humidity is the same as that over the EIO/EEP. The theoretical profile is a very good approximation to observed profile over EIO and EWP

where $m = H_T/H_1$ is the ratio of the density scale height H_T to the water vapor scale height H_1 ; and \bar{q}_s is air specific humidity at the surface. As shown in Fig. 12, this theoretical profile represents observed monthly or seasonal mean state very realistically.

The basic state specific humidity in any arbitrary vertical layer between p_i and p_j is a function of SST only and can be obtained readily by integrating Eq. (32).

Numerical scheme

The model is solved in an aqua-planet channel between 40°S and 40°N on a spherical coordinate by returning

the dimension of Eqs. (1)–(9) and converting them to the spherical coordinate. The parallel β -channel model on spherical coordinate (with β at the equator) is also tested and has nearly identical solutions. The zonal boundary condition is periodic. At the meridional boundaries, the fluxes of mass, momentum, and heat normal to the boundaries vanish. The typical values for the model parameters used in numerical calculations are listed in Table 1.

The numerical scheme derived by Lin and Rood (1997) is adopted. The spatial resolution is 4° longitude by 2° latitude. The time step is 10 min in the B–M simulation and 5 min in the Kuo simulation. Sensitivity tests are performed using a finer horizontal resolution. The major dynamical features remain unaffected to the change in horizontal resolution if we decrease the time step and add horizontal diffusion terms.

Appendix 2

Justification of positive-only precipitation

In this model, a resting background atmosphere is assumed for simplicity. Under this assumption, perturbation motion is also the total motion. For the Kuo scheme, the moisture convergence equals the total moisture convergence. Thus, the positive moisture convergence corresponds to the total precipitation, while negative moisture convergence corresponds to no precipitation. For the Betts–Miller scheme, the total precipitation can be expressed as:

$$Pr = (q_{tot} - \bar{q})/\tau \quad (33)$$

where q_{tot} is the total column-integrated moisture and \bar{q} is the column-integrated reference moisture. The total column-integrated moisture can be further decomposed into perturbation column-integrated moisture q and basic state column-integrated moisture \bar{q} , $q_{tot} = q + \bar{q}$. The column-integrated moisture reference \bar{q} can also be decomposed into the mean part \hat{q} and the perturbation part $\tilde{q} = \alpha\Phi$. By assuming that the basic state is convective neutral ($\bar{q} = \hat{q}$), the total precipitation is determined by the anomalous field, which only the positive anomaly ($q - \tilde{q}(T) > 0$) would produce precipitation. Therefore, the use of positive only precipitation in the B–M scheme is also reasonable.

References

- Adames ÁF, Kim D (2015) The MJO as a dispersive, convectively coupled moisture wave: theory and observations. *J Atmos Sci*. doi:10.1175/JAS-D-15-0170.1
- Adames ÁF, Wallace JM (2014) Three-dimensional structure and evolution of the vertical velocity and divergence fields in the MJO. *J Atmos Sci* 71:4661–4681. doi:10.1175/JAS-D-14-0091.1
- Andersen JA, Kuang Z (2012) Moist static energy budget of MJO-like disturbances in the atmosphere of a zonally symmetric aquaplanet. *J Clim* 25:2782–2804. doi:10.1175/JCLI-D-11-00168.1
- Benedict JJ, Maloney ED, Sobel AH, Frierson DMW (2014) Gross moist stability and MJO simulation skill in three full-physics GCMs. *J Atmos Sci* 71:3327–3349. doi:10.1175/JAS-D-13-0240.1
- Betts AK (1986) A new convective adjustment scheme: part I—observational and theoretical basis. *Quart J R Meteorol Soc* 112:677–691
- Betts A, Miller M (1986) A new convective adjustment scheme: Part II—single column tests using GATE wave, BOMEX, ATEX and arctic air-mass data sets. *Q J R Meteorol Soc* 112:693–709
- Bony S, Emanuel KA (2005) On the role of moist processes in tropical intraseasonal variability: cloud-radiation and moisture–convection feedbacks. *J Atmos Sci* 62:2770–2789. doi:10.1175/JAS3506.1
- Emanuel KA (1987) An air–sea interaction model of intraseasonal oscillations in the tropics. *J Atmos Sci* 44:2324–2340. doi:10.1175/1520-0469(1987)044<2324:AASIMO>2.0.CO;2
- Flatau M, Flatau PJ, Phoebus P, Niiler PP (1997) The feedback between equatorial convection and local radiative and evaporative processes: the implications for intraseasonal oscillations. *J Atmos Sci* 54:2373–2386
- Frierson DM, Majda AJ, Pauluis OM (2004) Large scale dynamics of precipitation fronts in the tropical atmosphere: a novel relaxation limit. *Commun Math Sci* 2:591–626
- Fu X, Wang B (2004) The boreal-summer intraseasonal oscillations simulated in a hybrid coupled atmosphere–ocean model*. *Mon Weather Rev* 132:2628–2649
- Fu X, Wang B (2009) Critical roles of the stratiform rainfall in sustaining the Madden–Julian oscillation: GCM experiments*. *J Clim* 22:3939–3959. doi:10.1175/2009JCLI2610.1
- Fuchs Ž, Raymond DJ (2002) Large-scale modes of a nonrotating atmosphere with water vapor and cloud-radiation feedbacks. *J Atmos Sci* 59:1669–1679. doi:10.1175/1520-0469(2002)059<1669:LSMOAN>2.0.CO;2
- Gill AE (1980) Some simple solutions for heat-induced tropical circulation. *Quart J Roy Meteorol Soc* 106:447–462
- Grabowski WW, Moncrieff M (2004) Moisture–convection feedback in the tropics. *Quart J R Meteorol Soc* 130:3081–3104
- Holloway CE, Woolnough SJ, Lister GMS (2013) The effects of explicit versus parameterized convection on the MJO in a large-domain high-resolution tropical case study: part I—characterization of large-scale organization and propagation*. *J Atmos Sci* 70:1342–1369. doi:10.1175/JAS-D-12-0227.1
- Hsu P-C, Li T (2012) Role of the boundary layer moisture asymmetry in causing the eastward propagation of the Madden–Julian oscillation*. *J Clim* 25:4914–4931. doi:10.1175/JCLI-D-11-00310.1
- Jiang X et al (2015) Vertical structure and physical processes of the Madden–Julian oscillation: exploring key model physics in climate simulations. *J Geophys Res: Atmos* 120:4718–4748
- Johnson RH, Rickenbach TM, Rutledge SA, Ciesielski PE, Schubert WH (1999) Trimodal characteristics of tropical convection. *J Clim* 12:2397–2418. doi:10.1175/1520-0442(1999)012<2397:TCOTC>2.0.CO;2
- Kang I-S, Liu F, Ahn M-S, Yang Y-M, Wang B (2013) The role of SST structure in convectively coupled Kelvin–Rossby waves and its implications for MJO formation. *J Clim* 26:5915–5930
- Khouider B, Majda AJ (2006) A simple multicloud parameterization for convectively coupled tropical waves: part I—linear analysis. *J Atmos Sci* 63:1308–1323. doi:10.1175/JAS3677.1
- Khouider B, Majda AJ (2007) A Simple multicloud parameterization for convectively coupled tropical waves: part II—nonlinear simulations. *J Atmos Sci* 64:381–400. doi:10.1175/JAS3833.1

- Kikuchi K, Takayabu YN (2004) The development of organized convection associated with the MJO during TOGA COARE IOP: trimodal characteristics. *Geophys Res Lett* 31:L10101
- Kiladis GN, Straub KH, Haertel PT (2005) Zonal and vertical structure of the Madden–Julian oscillation. *J Atmos Sci* 62:2790–2809
- Kim D, Kug J-S, Sobel AH (2014) Propagating versus nonpropagating Madden–Julian oscillation events. *J Clim* 27:111–125. doi:10.1175/JCLI-D-13-00084.1
- Knutson TR, Weickmann KM, Kutzbach JE (1986) Global-scale intraseasonal oscillations of outgoing longwave radiation and 250 mb zonal wind during Northern Hemisphere summer. *Mon Weather Rev* 114:605–623. doi:10.1175/1520-0493(1986)114<0605:GSI000>2.0.CO;2
- Krishnamurti TN, Oosterhof DK, Mehta AV (1988) Air–sea interaction on the time scale of 30 to 50 days. *J Atmos Sci* 45:1304–1322. doi:10.1175/1520-0469(1988)045<1304:AIOTTS>2.0.CO;2
- Kuang Z (2008) A moisture–stratiform instability for convectively coupled waves. *J Atmos Sci* 65:834–854. doi:10.1175/2007JAS2444.1
- Lau KM, Peng L (1987) Origin of low-frequency (intraseasonal) oscillations in the tropical atmosphere: part I—basic theory. *J Atmos Sci* 44:950–972. doi:10.1175/1520-0469(1987)044<0950:OOLF0I>2.0.CO;2
- Lee M-I, Kang I-S, Kim J-K, Mapes BE (2001) Influence of cloud-radiation interaction on simulating tropical intraseasonal oscillation with an atmospheric general circulation model. *J Geophys Res* 106(D13):14219–14233
- Lee S-S, Wang B, Waliser DE, Neena JM, Lee J-Y (2015) Predictability and prediction skill of the boreal summer intraseasonal oscillation in the Intraseasonal Variability Hindcast Experiment. *Clim Dyn* 45:2123–2135
- Lin J-L, Mapes BE (2004) Radiation budget of the tropical intraseasonal oscillation. *J Atmos Sci* 61:2050–2062. doi:10.1175/1520-0469(2004)061<2050:RBOTTI>2.0.CO;2
- Lin SJ, Rood RB (1997) An explicit flux-form semi-lagrangian shallow-water model on the sphere. *Quart J R Meteorol Soc* 123:2477–2498
- Lin J, Mapes B, Zhang M, Newman M (2004) Stratiform precipitation, vertical heating profiles, and the Madden–Julian oscillation. *J Atmos Sci* 61:296–309. doi:10.1175/1520-0469(2004)061<0296:SPVHPA>2.0.CO;2
- Liu F, Wang B (2012a) A frictional skeleton model for the Madden–Julian oscillation*. *J Atmos Sci* 69:2749–2758. doi:10.1175/JAS-D-12-020.1
- Liu F, Wang B (2012b) A model for the interaction between 2-day waves and moist Kelvin waves. *J Atmos Sci* 69:611–625. doi:10.1175/JAS-D-11-0116.1
- Liu F, Wang B (2013) Impacts of upscale heat and momentum transfer by moist Kelvin waves on the Madden–Julian oscillation: a theoretical model study. *Clim Dyn* 40:213–224
- Liu F, Wang B (2016) Effects of moisture feedback in a frictional coupled Kelvin–Rossby wave model and implication in the Madden–Julian oscillation dynamics. *Clim Dyn*:1–10
- Madden RA, Julian PR (1972) Description of global-scale circulation cells in the tropics with a 40–50 day period. *J Atmos Sci* 29:1109–1123. doi:10.1175/1520-0469(1972)029<1109:DOGS CC>2.0.CO;2
- Majda AJ, Biello JA (2004) A multiscale model for tropical intraseasonal oscillations. *Proc Natl Acad Sci USA* 101:4736–4741
- Majda AJ, Stechmann SN (2009) The skeleton of tropical intraseasonal oscillations. *Proc Natl Acad Sci* 106:8417–8422
- Maloney ED (2009) The moist static energy budget of a composite tropical intraseasonal oscillation in a climate model. *J Clim* 22:711–729. doi:10.1175/2008JCLI2542.1
- Maloney ED, Sobel AH, Hannah WM (2010) Intraseasonal variability in an aquaplanet general circulation model. *J Adv Model Earth Syst* 2:5
- Mapes BE (2000) Convective inhibition, subgrid-scale triggering energy, and stratiform instability in a toy tropical wave model. *J Atmos Sci* 57:1515–1535. doi:10.1175/1520-0469(2000)057<1515:CISSTE>2.0.CO;2
- Mori M, Watanabe M (2008) The growth and triggering mechanisms of the PNA: a MJO–PNA coherence. *J Meteorol Soc Jpn Ser II* 86:213–236
- Nakazawa T (1988) Tropical super clusters within intraseasonal variations over the western Pacific. *J Meteorol Soc Jpn* 66:823–839
- Neelin JD, Yu J-Y (1994) Modes of tropical variability under convective adjustment and the Madden–Julian oscillation: part I—analytical theory. *J Atmos Sci* 51:1876–1894. doi:10.1175/1520-0469(1994)051<1876:MOTVUC>2.0.CO;2
- Neelin JD, Held IM, Cook KH (1987) Evaporation–wind feedback and low-frequency variability in the tropical atmosphere. *J Atmos Sci* 44:2341–2348. doi:10.1175/1520-0469(1987)044<2341:EWFA LF>2.0.CO;2
- Neena JM, Lee JY, Waliser D, Wang B, Jiang X (2014) Predictability of the Madden–Julian oscillation in the Intraseasonal Variability Hindcast Experiment (ISVHE). *J Clim* 27:4531–4543. doi:10.1175/JCLI-D-13-00624.1
- Pritchard MS, Bretherton CS (2014) Causal evidence that rotational moisture advection is critical to the superparameterized Madden–Julian oscillation. *J Atmos Sci* 71:800–815. doi:10.1175/JAS-D-13-0119.1
- Pritchard MS, Yang D (2016) Response of the superparameterized Madden–Julian oscillation to extreme climate and basic-state variation challenges a moisture mode view. *J Climate* 29:4995–5008
- Raymond DJ (2001) A new model of the Madden–Julian oscillation. *J Atmos Sci* 58:2807–2819. doi:10.1175/1520-0469(2001)058<2807:ANMOTM>2.0.CO;2
- Raymond DJ, Fuchs Ž (2009) Moisture modes and the Madden–Julian oscillation. *J Clim* 22:3031–3046. doi:10.1175/2008JCLI2739.1
- Rui H, Wang B (1990) Development characteristics and dynamic structure of tropical intraseasonal convection anomalies. *J Atmos Sci* 47:357–379. doi:10.1175/1520-0469(1990)047<0357:DCA DSO>2.0.CO;2
- Seo K-H, Wang W (2010) The Madden–Julian oscillation simulated in the NCEP climate forecast system model: the importance of stratiform heating. *J Clim* 23:4770–4793. doi:10.1175/2010JCLI2983.1
- Sobel A, Maloney E (2012) An idealized semi-empirical framework for modeling the Madden–Julian oscillation. *J Atmos Sci* 69:1691–1705
- Sobel A, Maloney E (2013) Moisture modes and the eastward propagation of the MJO. *J Atmos Sci* 70:187–192. doi:10.1175/JAS-D-12-0189.1
- Sperber KR (2003) Propagation and the vertical structure of the Madden–Julian oscillation. *Mon Weather Rev* 131:3018–3037. doi:10.1175/1520-0493(2003)131<3018:PATVSO>2.0.CO;2
- Tian B, Waliser DE, Fetzer EJ, Lambrigtsen BH, Yung YL, Wang B (2006) Vertical moist thermodynamic structure and spatial–temporal evolution of the MJO in AIRS observations. *J Atmos Sci* 63:2462–2485
- Tomasi C (1984) Vertical distribution features of atmospheric water vapor in the Mediterranean, Red Sea, and Indian Ocean. *J Geophys Res: Atmos* (1984–2012) 89:2563–2566
- Wang B (1988a) Comments on “an air–sea interaction model of intraseasonal oscillation in the tropics”. *J Atmos Sci* 45:3521–3525
- Wang B (1988b) Dynamics of tropical low-frequency waves: an analysis of the moist Kelvin wave. *J Atmos Sci* 45:2051–2065. doi:10.1175/1520-0469(1988)045<2051:DOTLFW>2.0.CO;2

- Wang B (2005) Theory. In: Lau WKM, Waliser DE (eds) *Intraseasonal variability in the atmosphere–ocean climate system*, 1st edn. Springer, Berlin, pp 307–360
- Wang B (2012) Theory. In: Lau WKM, Waliser DE (eds) *Intraseasonal variability in the atmosphere–ocean climate system*, 2nd edn. Springer, Berlin, pp 335–398
- Wang B, Li T (1994) Convective interaction with boundary-layer dynamics in the development of a tropical intraseasonal system. *J Atmos Sci* 51:1386–1400. doi:[10.1175/1520-0469\(1994\)051<1386:CIWBLD>2.0.CO;2](https://doi.org/10.1175/1520-0469(1994)051<1386:CIWBLD>2.0.CO;2)
- Wang B, Liu F (2011) A model for scale interaction in the Madden–Julian oscillation*. *J Atmos Sci* 68:2524–2536
- Wang B, Rui H (1990a) Dynamics of the coupled moist Kelvin–Rossby wave on an equatorial β -plane. *J Atmos Sci* 47:397–413. doi:[10.1175/1520-0469\(1990\)047<0397:DOTCMK>2.0.CO;2](https://doi.org/10.1175/1520-0469(1990)047<0397:DOTCMK>2.0.CO;2)
- Wang B, Rui H (1990b) Synoptic climatology of transient tropical intraseasonal convection anomalies: 1975–1985. *Meteorol Atmos Phys* 44:43–61
- Wang B, Xie X (1998) Coupled modes of the warm pool climate system: Part I: the role of air–sea interaction in maintaining Madden–Julian oscillation. *J Clim* 11:2116–2135. doi:[10.1175/1520-0442-11.8.2116](https://doi.org/10.1175/1520-0442-11.8.2116)
- Wang B, Zhang Q (2002) Pacific–East Asian teleconnection: part II—how the Philippine Sea anomalous anticyclone is established during El Niño development*. *J Clim* 15:3252–3265. doi:[10.1175/1520-0442\(2002\)015<3252:PEATPI>2.0.CO;2](https://doi.org/10.1175/1520-0442(2002)015<3252:PEATPI>2.0.CO;2)
- Wheeler MC, Hendon HH (2004) An all-season real-time multivariate MJO index: development of an index for monitoring and prediction. *Mon Weather Rev* 132:1917–1932. doi:[10.1175/1520-0493\(2004\)132<1917:AARMMI>2.0.CO;2](https://doi.org/10.1175/1520-0493(2004)132<1917:AARMMI>2.0.CO;2)
- Woolnough S, Slingo J, Hoskins B (2001) The organization of tropical convection by intraseasonal sea surface temperature anomalies. *Quart J R Meteorol Soc* 127:887–907
- Yang D, Ingersoll AP (2011) Testing the hypothesis that the MJO is a mixed Rossby–gravity wave packet. *J Atmos Sci* 68:226–239
- Yang D, Ingersoll AP (2013) Triggered convection, gravity waves, and the MJO: a shallow-water model. *J Atmos Sci* 70:2476–2486. doi:[10.1175/JAS-D-12-0255.1](https://doi.org/10.1175/JAS-D-12-0255.1)
- Zhang C (2005) Madden–Julian oscillation. *Rev Geophys* 43:1–36
- Zhang C, Ling J (2012) Potential vorticity of the Madden–Julian oscillation. *J Atmos Sci* 69:65–78. doi:[10.1175/JAS-D-11-081.1](https://doi.org/10.1175/JAS-D-11-081.1)